Estimation of the local instantaneous heat flux inside a pulsating heat pipe for space applications

L Cattani[1], L Pagliarini[1], F Bozzoli[1], M Mameli[2], S Filippeschi[2], M Marengo[3], L Pietrasanta[3], N Miché[3], D Mangini[4]

[1]Department of Engineering and Architecture, University of Parma, Parma, Italy
[2]Department of Energy, Systems Land and Construction Engineering, University of Pisa, Pisa, Italy
[3]Advanced Engineering Centre, University of Brighton, Brighton, UK
[4]Cosine Remote Sensing BV, 2171 AH Sassenheim, The Netherlands

Corresponding author: luca.cattani1@unipr.it ORCID ID: 0000-0002-0287-4452

Abstract. Pulsating Heat Pipes (PHP) are promising and effective passive two-phase heat transfer devices in terms of high heat transfer capability, efficient thermal control, adaptability and low cost and therefore they have been extensively studied in the last years. Many authors have estimated the heat fluxes at the evaporator and at the condenser area only in terms of the average values based on first principle considerations. In the present study the application of an inverse analysis technique to experimental infrared temperature data is proposed to investigate the local convective heat flux for forced convection flow inside these devices along the adiabatic zone. A PHP specifically designed to be hosted on board the heat transfer host of the International Space Station was tested in microgravity during the 67th Parabolic Flight Campaign organized by the European Space Agency. The device consists of an aluminium tube closed in a loop with 14 turns in the evaporator section, 3 mm inner diameter, half filled with FC-72 fluid. The external temperatures of the device are measured in the adiabatic zone with a high-speed infrared camera (50 Hz, 1280x1024 pixels). The images are thereafter post-processed and adopted as input data for the solution of the inverse heat conduction problem in the pipe wall (Tikhonov regularisation method) to extrapolate time-varying local heat fluxes on the tube internal surface in contact with the fluid.

1. Introduction

One of the main challenges of technological development is to solve thermal management problems and save energy at the same time. A primary dare is constituted for example by the cooling of the electronic components considering their ever-increasing thermal power density: these requirements feed the race for the rising of innovative technologies that guarantee the coupling between high thermal performance and reduced dimensions [1]. A rapidly expanding field of research certainly concerns space applications that additionally are characterised by extreme environmental conditions, strict constrains in terms of compactness, reliability and the need to dissipate efficiently heat in microgravity conditions [2,3].

A high potential response to these needs is represented by a promising solution in the field of passive two-phase heat transfer devices: the Pulsating Heat Pipes (PHPs). They were patented in the 1990s [4]

and they quickly attracted the interest of both researchers and companies thanks to the elevated heat transfer capability, efficient thermal control, adaptable geometry and low cost. They are essentially constituted by a capillary tube bent several times between heating and cooling sections, called evaporator and condenser, respectively. The pipe is partially filled with working fluid which resides internally as an alternance of liquid slugs and vapor plugs whose oscillating motion is purely thermally induced [5]. Despite their unique advantages, the thermo-fluid dynamics governing the internal two-phase oscillating flow is very complex because many processes, such as capillary actions and phase changes, are involved; therefore, the behaviour of these devices is not fully understood yet. In order to analyse and deeply understand the fundamental principles of their thermal behaviour, many studies have been carried out in recent years [6-10].

Almost all the studies performed with the aim of analysing the principles of thermal operation of PHPs, involved the study of the average heat transfer rate over the entire heat transfer area (evaporator or condenser) or the study of the overall thermal resistance of the system. However, the knowledge of local heat transfer dynamics is crucial for a better comprehension of the fundamental physical mechanisms ruling the behavior of these devices and for their optimization.

For these reasons in the present study the application of an inverse analysis technique to experimental infrared temperature data is proposed to estimate the convective heat flux inside PHPs. The calculation is based on the solution of the Inverse Heat Conduction Problem (IHCP) within the wall domain of the pipe: the input data are represented by the infrared temperature maps acquired on the outer pipe wall. Although, this solution technique allows to estimate the local heat flux on the inner pipe wall, it presents some drawbacks due to the ill-posed nature of inverse problems which are very sensitive to small disturbances in the input data. To overcome this issue, many techniques based on experimental data processing have been suggested and validated in the literature (e.g., regularization, filtering, function specification, probabilistic and iterative methods) [11-13].

Among the numerous possible applications of this approach, the estimation of the temperature, the heat flux, or the convective heat transfer coefficient distributions on the internal wall of a duct, using only the external wall temperature distribution, is very appealing. For this reason, it is possible to find several studies in literature that face this argument either about the investigation of the heat transfer mechanisms either about industrial applications to monitor productive processes. Among the different studies about inverse heat transfer approach in pipes we can find different geometrical schematization of the physical problem, i.e. 0D [18], 1D [17], 2D [14,15], 2D-axialsymmetric [19], 3D [16] and both stationary [15-17] and transient studies [14,18,19].

In the present work to estimate the time-varying convective heat flux at the fluid-internal wall interface, Tikhonov's method of regularization has been adopted [20]. The local heat flux of a PHP especially designed for space applications and tested during the 67th Parabolic Flight Campaign (PFC) promoted by the European Space Agency (ESA), has been evaluated in microgravity conditions.

2. Experimental setup

The PHP is composed of an annealed aluminium (6060 alloy) tube with an inner and outer diameter of 3 and 5 mm, respectively.

The closed loop is folded in a staggered 3D configuration with 14 turns (8 mm bending radius) in the evaporator zone, as shown in figures 1 and 2. It is essentially constituted by 3 sections, including evaporator, condenser and adiabatic.

The PHP is placed in a vertical position (90 deg) with the heated section (i.e. the evaporator) at the bottom as shown in figure 2.

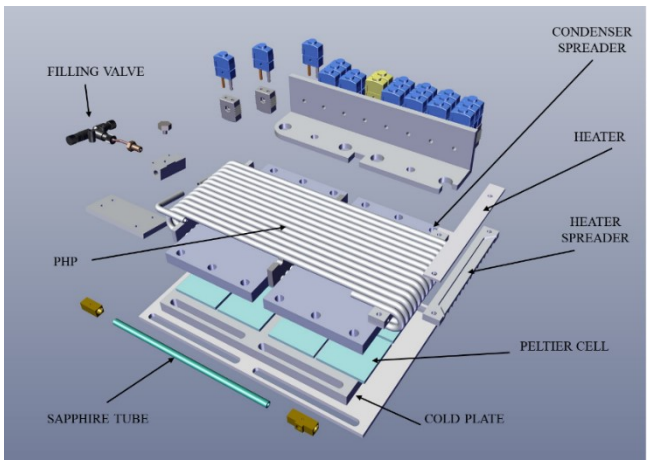

Figure 1. Sketch of the studied PHP.

To obtain a uniform temperature of the evaporator, two aluminium heat spreaders (100x12x10mm) are brazed on the tube in the evaporator zone (see figures 1 and 2), holding two ceramic Ohmic heaters (Innovacera®, electrical resistance 18Ω ±10%). The heating power is given by a power supply (GW-Instek®, PSH-6006A) in the range from 10 W to 210 W.

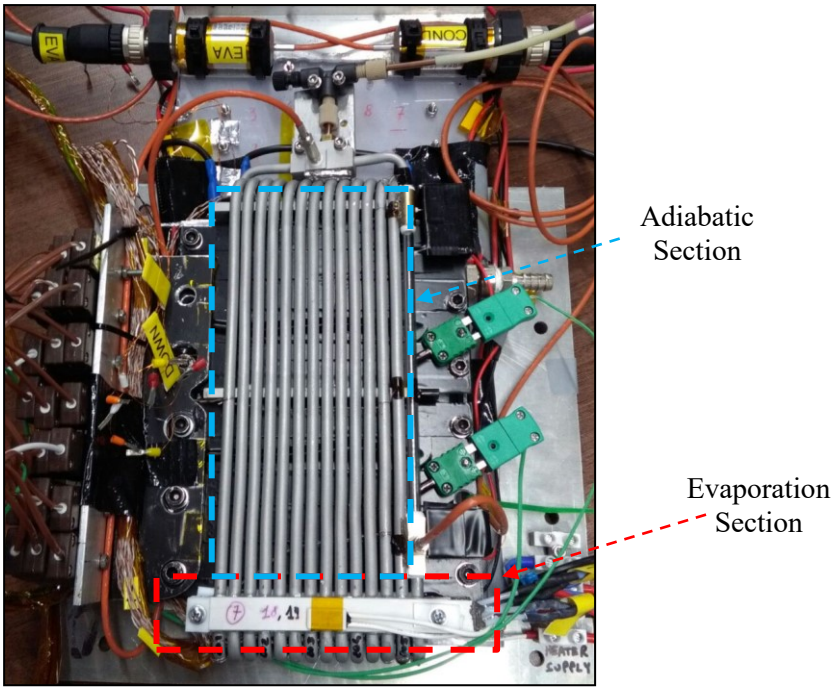

Figure 2. Picture of the experimental setup.

The temperature of the evaporator is measured through 5 type-T thermocouples placed between the evaporator spreader and the heater. Moreover, to detect and prevent overheating, 1 type-T thermocouple was attached on the sheet heater. The condenser zone is embedded between two aluminium heat spreaders (80x120x10mm), cooled down by means of a Peltier cell system (8 Peltier cells by Adaptive Thermal Management®, ETH-127-14-11-S; control system by Meertstetter Engineering®, TEC 1123) coupled with a cold plate temperature control system loop (Aavid Thermalloy®). The temperature at the condenser is monitored by six thermocouples placed between the Peltier cold side and the condenser

aluminium heat spreader and two located on the condenser heat spreader. The environmental temperature was checked with another thermocouple.

The fluid-to-wall heat flux has been estimated in the region between the evaporator and the condenser (adiabatic section) since it is the only portion of the device accessible to the infrared camera.

The channels within the adiabatic section were coated with uniform and high emissivity opaque paint and the temperature is acquired by means of a highspeed and high resolution MWIR camera (AIM® TEC-MMG from ESA/ ESTEC, 50 Hz, 1280x1024 pixels). A portion of the PHP adiabatic section, highlighted in green in figure 3, is framed by the Infrared camera. When using an infrared camera, care should be taken in temperature measurement if the targeted surface is not normal to the optical axis of the camera because the emissivity of real surfaces is directional. Since the IR measurements are not reliable over a certain maximum viewing angle from the camera lens (> 30°), the analysis is carried out only on 10 of the 13 aluminum channels and only the central part of each tube was considered. Under these conditions the surface displayed was considered as a diffuse grey emitter [22]. Figure 3 additionally shows the reference for the aluminum channels numeration. The thermographic images are then processed by perspective algorithms [21] in Matlab® environment.

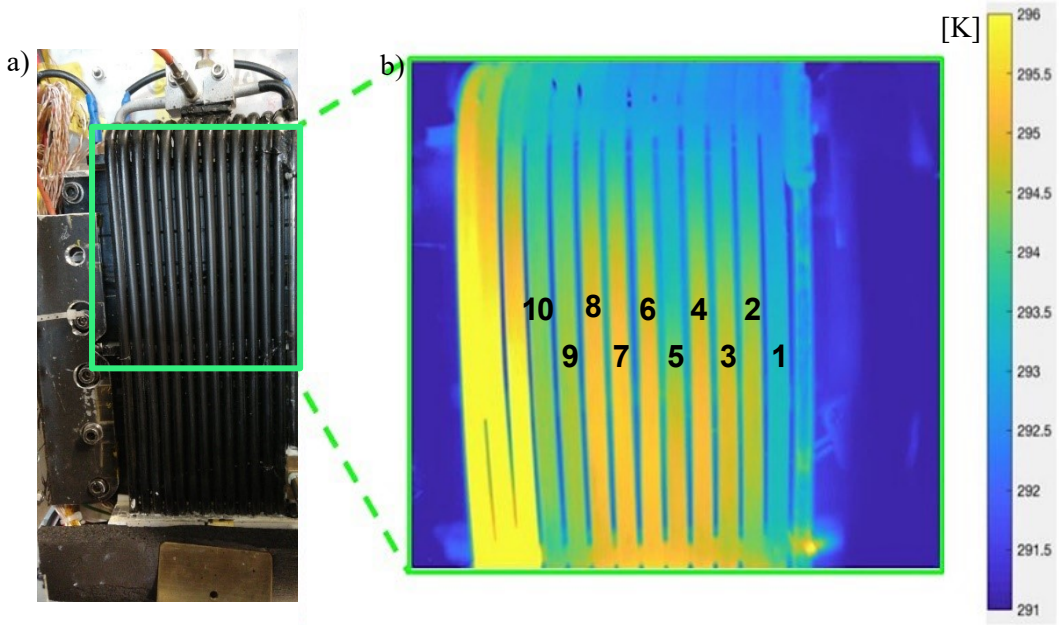

Figure 3. a) Analyzed PHP section; b) a representative thermographic image.

For calibration purposes, preliminary measurements were performed in situ to evaluate the effective emissivity of the coating. Moreover, the value of the emissivity was checked by comparing the temperature measurement results on the IR thermal images with the measurements from seven thermocouples located on the tube external wall in different positions in the portion between the condenser and the evaporator. The PHP was first vacuumed (down to 10^{-6} mbar) and then partially filled through the valve shown in figure 1 with degassed FC-72 (filling ratio = 50 ± 1% vol.). The test rig was then mounted on an Airbus A310 and 93 parabolic trajectories were performed over three days of flight. Each parabola is composed by a first hyper-gravity period (20 s ± 2 s at 1.8g), the microgravity period (20 s ± 2 s at 0.01 g) and a second hyper-gravity period equal to the first. To study the thermal performance in microgravity conditions the device is heated up at the desired power level before the microgravity period, and the power level is kept constant. The microgravity period duration (about 20 s) is not enough to reach a pseudo-steady state (i.e. when the mean value of the oscillating temperature signal is constant in time), nevertheless it can give fundamental information about the thermal behaviour of the studied device in microgravity conditions. Further details about experimental setup can be found in a previous work of the Authors [23].

3. Estimation Procedure

Starting from the temperature distribution of the external wall surface of the tube, it is possible to estimate the local convective heat flux at the fluid-internal wall interface by solving the inverse heat conduction problem in the channel wall. In the present work one of the most employed regularization techniques, the Tikhonov method, is adopted [20]. The test section, represented by each of the channels shown in figure 3 was modelled as a 1-D solid domain on the basis of two assumptions that are discussed and verified further on in the text: the temperature gradient is almost negligible along the circumferential coordinate and therefore the problem can be considered 2D-axysimmetric; the axial component of the heat flux in the pipe wall represented by the Laplacian of the temperature along the axial coordinate is one order magnitude lower than the time-variant component of the heat flux and thus can be neglected as first approximation. For these reasons the 2D solid domain represented in figure 4 is assumed to be uniformly heated along the circumferential coordinate.

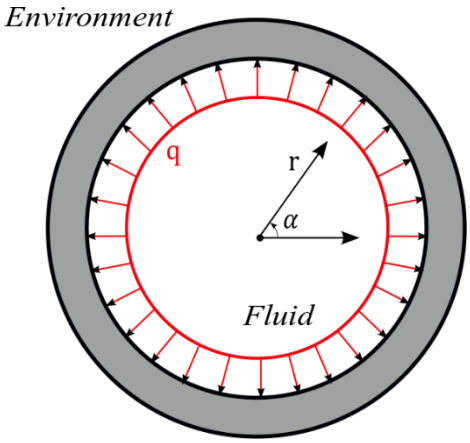

Figure 4. Geometrical domain with coordinate system.

Under the above described conditions, the energy balance equation in the solid domain is expressed as follows:

$$k\nabla^2 T = \rho c_p \frac{\partial T}{\partial t} \tag{1}$$

where T is the temperature, t is the time and k, ρ and c_p are the channel thermal conductivity, density, and specific heat, respectively. The following two boundary conditions, applied on the internal surface (eq. (2a)) and on the external surface (eq. (2b)) of the pipe, completed the energy balance equation:

$$-k\frac{\partial T}{\partial r}\bigg|_{r=r_{int}} = q \tag{2a}$$

$$\frac{\partial T}{\partial r}\bigg|_{r=r_{ext}} = -\frac{(T - T_{env})}{R_{env}} \tag{2b}$$

The wall thermal conductivity of the aluminium channel k was certified by the manufacturer to be equal to 201 W/mK at 300 K and the overall heat-transfer resistance R_{env} between the channel wall and the surrounding environment, which was assumed to be known in the inverse problem considered here, was assumed equal to 0.1 m^2K/W, which is a representative value for air natural convection with radiative heat transfer towards the environment [24]. The heat conduction problem, according to [11], can be written in the discrete domain as follows:

$$\mathbf{T} = \mathbf{Xq} + \mathbf{T_{q=0}} \tag{3}$$

where **T** is the vector of the discrete temperature data at the external pipe surface, **q** is the heat flux vector at the fluid-internal wall interface assumed to be uniform for all the angular coordinates, $\mathbf{T_{q=0}}$ is a constant term that is determined by imposing a null heat flux and **X** is the sensitivity matrix. The temperature and heat flux vectors **T** and **q** can be written as:

$$\mathbf{T} = \begin{bmatrix} T_1 \\ T_2 \\ \vdots \\ T_{N-1} \\ T_N \end{bmatrix}, \quad \mathbf{q} = \begin{bmatrix} q_1 \\ q_2 \\ \vdots \\ q_{N-1} \\ q_N \end{bmatrix} \tag{4a, b}$$

where N is the total number of time steps at which the temperature on the external pipe's surface is evaluated. The sensitivity matrix **X** and the $\mathbf{T_{q=0}}$ values, for the problem under test, can be calculated numerically [25] using the two-point difference approach:

$$X_{i,j} = \frac{T_i(q_1, q_2, \ldots, q_j + \Delta q, \ldots, q_N) - T_i(q_1, q_2, \ldots, q_j, \ldots, q_N)}{\Delta q} \tag{5}$$

$$T_{q=0,i} = T_i(q_1 = 0, q_2 = 0, \ldots, q_j = 0, \ldots, q_N = 0) \tag{6}$$

where T_i is the temperature on the external pipe's surface evaluated for i^{th} time step obtained by numerically solving the physical problem, represented by equations (1-2), by the finite element method implemented in COMSOL Multiphysics® environment and imposing an internal heat flux distribution **q** as defined by equation (3). In an analogous way, the constant vector $\mathbf{T_{q=0}}$ was determined by imposing a null heat flux. In the inverse formulation, this computed temperature distribution **T** is forced to match the experimental temperature distribution **Y** by tuning the convective heat-flux distribution on the internal wall side **q**. The matching of the two temperature distributions could be easily performed under a least square approach. However, due to the ill-posed nature of the problem, the least square solution is generally dominated by noise, and some type of regularisation is required. In this work the Tikhonov regularisation method allows to reformulate the original problem as a well-posed problem that consists of minimising the following objective function:

$$f(\boldsymbol{q}) = \left\|\mathbf{Y} - \mathbf{Xq} - \mathbf{T_{q=0}}\right\|_2^2 + \lambda^2 \|\mathbf{Lq}\|_2^2 \tag{7}$$

where $\| \quad \|_2^2$ stands for the square of the 2-norm, λ is the regularisation parameter, **L** is the derivative operator and **T** is the distribution of the external surface temperature derived from a direct numerical solution of the problem obtained by imposing a given convective heat flux distribution on the internal wall side **q**. Often, **L** is the zero, first or second derivative operator [11]: in this work the zero-order derivative formulation was chosen. The function expressed in equation (7) represents a trade-off between two optimisation processes: first, the fidelity of the fit and second, the smoothness or the stability of the solution. The choice of a proper regularisation parameter requires a good balance between the size of the residual norm and the size of the solution norm: in the present work the L-curve method [26] determines the regularization parameter by locating the 'elbow' in a log-log plot of the norm of the regularized solution versus the corresponding residual norm, thus obtaining the balance above required. From a computational point of view, the 'corner' is the point on the L-curve where the curvature is maximised [26].

4. Validation of the estimation procedure

To validate this procedure, synthetic temperature data were generated by solving the direct problem with a known distribution of convective heat flux q at the internal wall surface. This temperature distribution,

spoiled by random noise, was then used as the input data of the inverse problem. A Gaussian noise characterized by a standard deviation ranging from 0.01 K to 1 K was employed. The numerical model has been implemented within the COMSOL Multiphysics® environment: it considered a time interval of about 20 s with a time step of 20 ms. According to the expected results in the real cases, the convective heat flux q was considered with a distribution characterized by a significant variation with time:

$$q = A \cdot sin(t/0.5) \tag{8}$$

where A as representative value was chosen to be equal to $4 \cdot 10^3$ W/m^2 (see figure 5) that is in the range of the values obtained in the experimental tests. In figure 6a the temperature distribution obtained solving the direct problem with the heat flux given in figure 5 is shown, while in figure 6b the noisy temperature used as input data for the inverse problem for noise level σ_Y = 0.05K is shown.

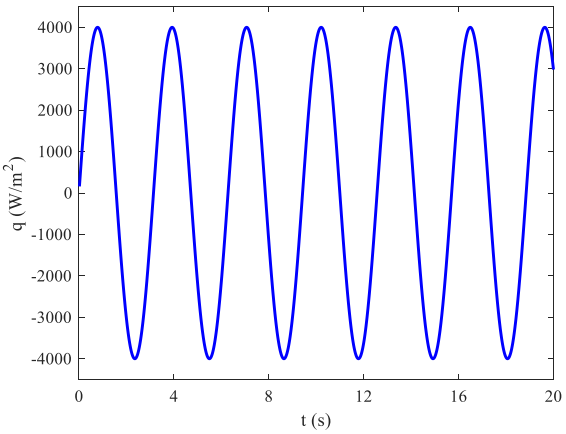

Figure 5. Synthetic heat flux distribution adopted in the validation procedure.

By solving the inverse problem, a convective heat flux distribution on the internal wall side was restored and compared to the data adopted to generate the input data: figure 7 shows the case of noise level σ_Y = 0.05K. To quantify the effectiveness of the applied approach at different signal-to-noise levels, an error analysis could be performed by plotting the estimation error, defined as follows:

$$E_q = \frac{\|q_{restored} - q_{exact}\|_2^2}{\|q_{exact}\|_2^2} \tag{9}$$

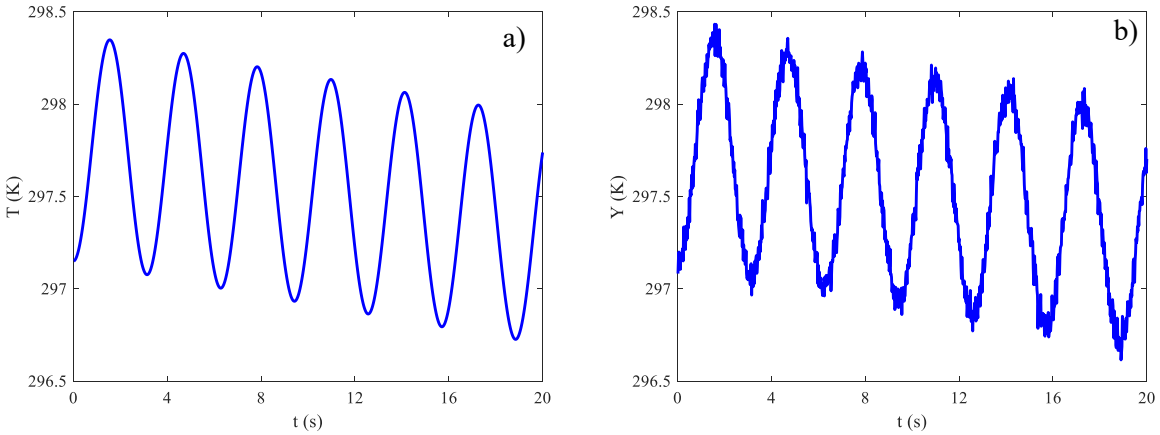

Figure 6. a) Temperature distribution obtained solving the direct problem; b) noisy temperature used as input data for the inverse problem for noise level σ_Y = 0.05K.

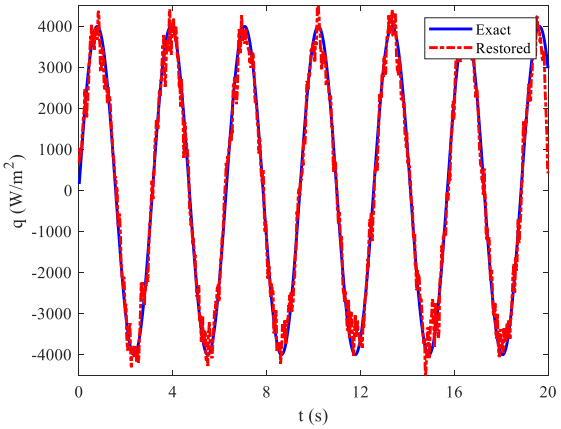

Figure 7. Exact and restored heat flux.

Figure 8 shows that the applied approach works satisfactorily in restoring the heat flux for noise level values lower than 0.3 K ($\sigma/(T_{max}-T_{min}) \approx 0.15$ in figure 8) while for greater noise level values, the restoration of the starting heat flux suffers from higher estimation errors. In figure 8 on the x-axis, it is reported the normalized noise level. It is computed dividing the noise variance by the maximum difference observable in the temperature signal. This value provides a more robust information about the estimation method performance since considering only the absolute noise value could bring to E_q significantly different depending on the extent of the signal variation.

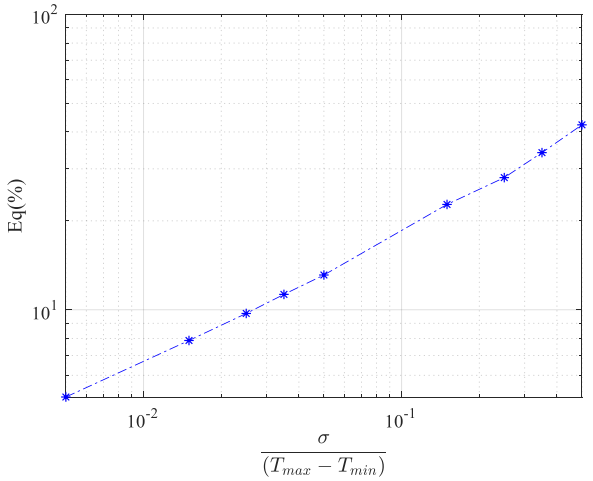

Figure 8. Estimation error on q at different noise level values.

5. Experimental results

The estimation procedure described above was then applied to the IR acquisitions obtained during the 67th Parabolic Flight Campaign (PFC) promoted by the European Space Agency (ESA). The heat flux distributions obtained with three different heat loads were analysed: i.e. 34, 100 and 202 W. The inverse approach has been applied to each of the ten PHP channels (see figure 3) for each heat load. Moreover, the procedure is repeated for several points along the axial coordinate of every channel. In figure 8 the temperature distribution along the axial coordinate (70 mm length) over a 20 seconds time span, is reported for the case of 100 W for the tube N°3 (see figure 3).

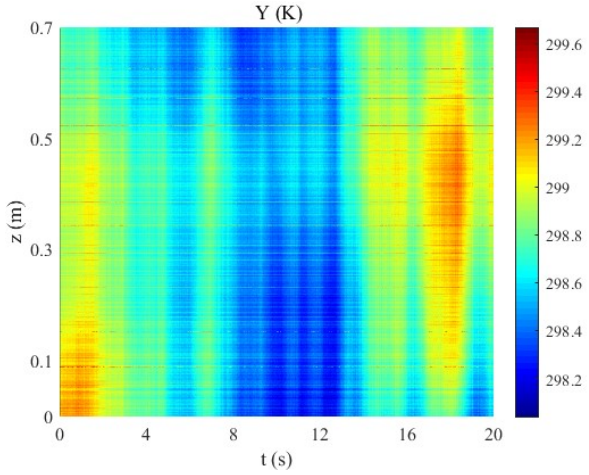

Figure 9. Wall temperature distribution for the case of heat load of 100 W for the tube N°3.

If the neglection of the angular component of the heat flux could be partially justified by considering figure 3 where it is possible to see that the temperature gradient is almost negligible along the circumferential coordinate for all the channels, the assumption that the axial component of the heat flux can be neglected, must be experimentally checked.

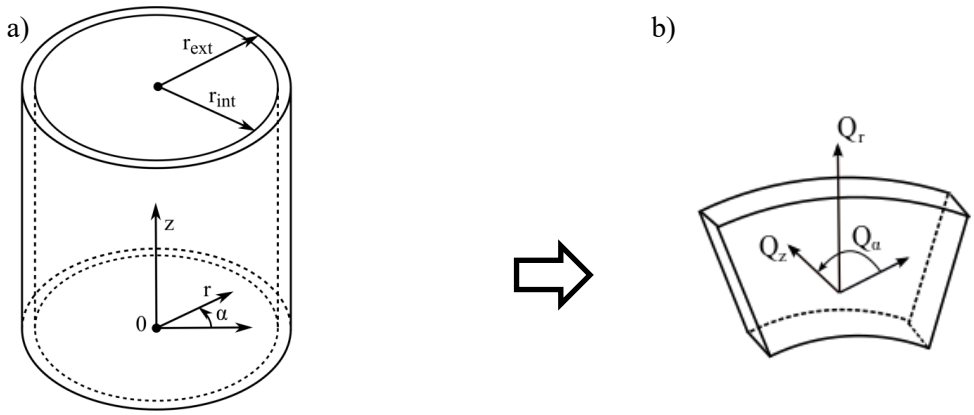

Figure 10. a) Test section coordinates system; b) infinitesimal cylindrical sector.

With reference to the infinitesimal cylindrical sector described in figure 10, the different components that contributes to the estimation of the heat flux at the internal surface can be expressed as:

$$Q_z = k\frac{\partial^2 T}{\partial z^2}\cdot\pi({r_{ext}}^2 - {r_{int}}^2) \tag{10a}$$

$$Q_t = \rho c_p\frac{\partial T}{\partial t}\cdot\pi({r_{ext}}^2 - {r_{int}}^2) \tag{10b}$$

$$Q_r = -\frac{(T - T_{env})}{R_{env}}\cdot 2\pi r_{ext} \tag{10c}$$

$$Q_\alpha = k\frac{\partial^2 T}{\partial \alpha^2}\cdot 2\pi \ln\left(\frac{r_{ext}}{r_{int}}\right) \tag{10d}$$

where Q is the power per unit length.

The different power components related to the temperature distribution shown in figure 9 are reported in figure 11. It is evident that the angular and axial components are negligible with respect to the time-variant component: this confirms that the two hypothesis proposed in Section 3 are acceptable and 1D Transient model of heat conduction will be adopted.

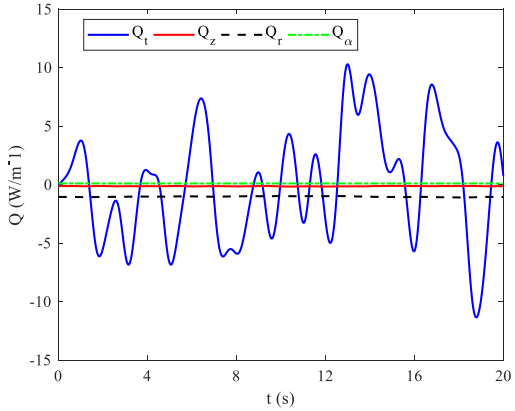

Figure 11. Different flux components for the case of heat load of 100 W and the tube N°3.

Figure 12a shows the L-curve for the same case reported in figure 9. The analysis reveals the presence of an elbow in correspondence of the section highlighted: among the suitable regularization parameter values it has been selected λ equal to $6.6 \cdot 10^{-5}$.

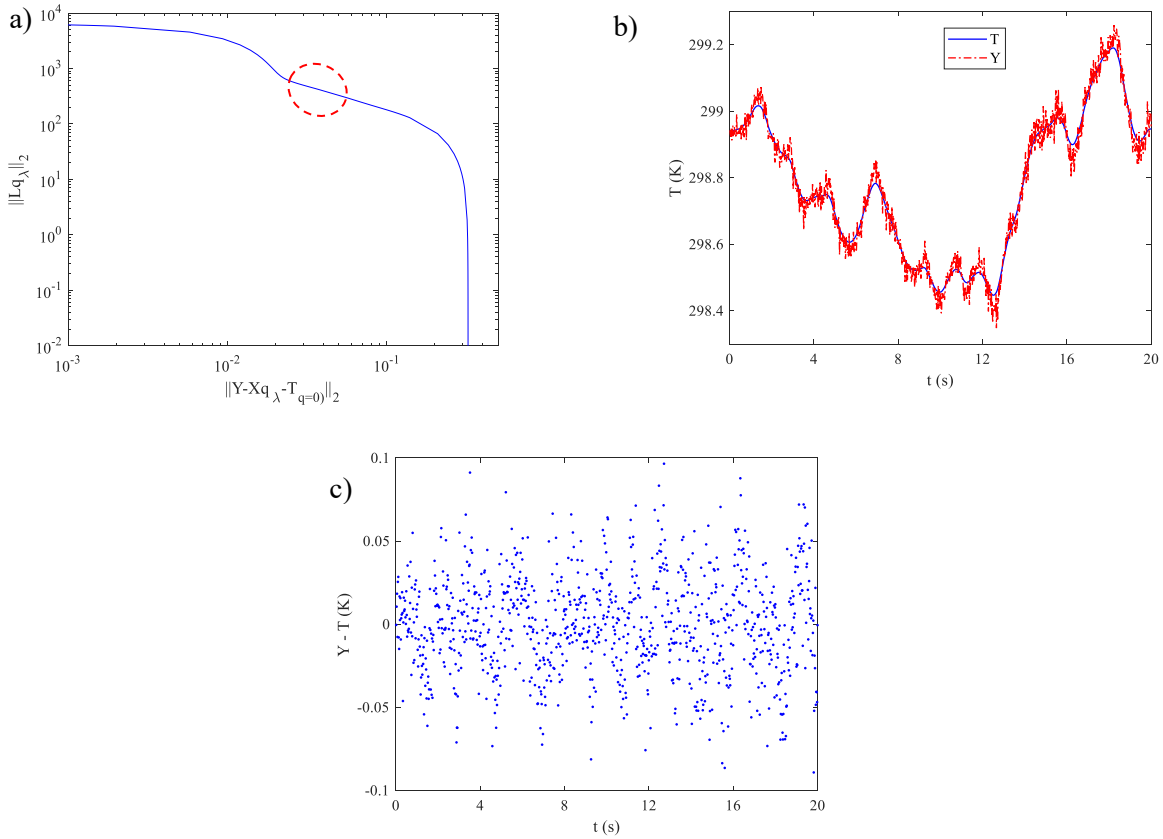

Figure 12. Case of heat load of 100 W for the tube N°3 at z=0.035m: a) L-curve in log–log scale; b) Experimental (Y) and reconstructed (T) temperature distribution; c) Residuals between the experimental (Y) and the reconstructed (T) temperature distribution.

In figure 12b, the reconstructed temperature distribution is compared with the experimental data: being the physical problem modelled as a 1-D solid domain, the time-variant temperature distribution measured in correspondence of only one axial coordinate value is considered (i.e. z =0.035m). Figure 12c shows that the residuals between the experimental and the computed temperature values are randomly distributed. This confirms that the simplified numerical model used in this study adequately describes the physical problem being tested. The distribution of the convective heat flux restored by the minimisation procedure presented above is reported in figure 13 for the case of heat load of 100 W for the tube N°3 for z=0.035m. Regarding the heat flux distribution, the following convention is adopted:

- positive heat flux, when the thermal energy is transferred from the fluid to the wall.
- negative heat flux, when the thermal energy is transferred from the wall to the fluid.

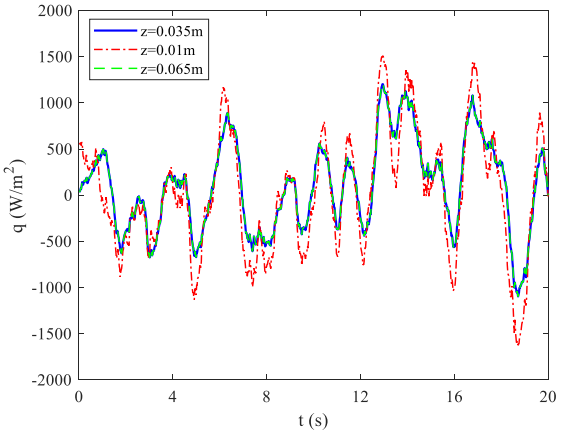

Figure 13. Heat flux distributions for the case of heat load of 100 W for the tube N°3

As further proof that the one-dimensional model adopted in this study adequately describes the investigated phenomenon, figure 13 shows the heat flux distribution for two other axial positions, i.e z=0.1m and z=0.65m. The three different distributions are comparable, thus confirming the goodness of the 1D model adoption. The heat flux distribution over time can provide useful information about the fluid dynamics inside the pipe. Positive heat fluxes correspond to the passage of hot vapor plugs and liquid slugs from the evaporator to the condenser.

a) b)

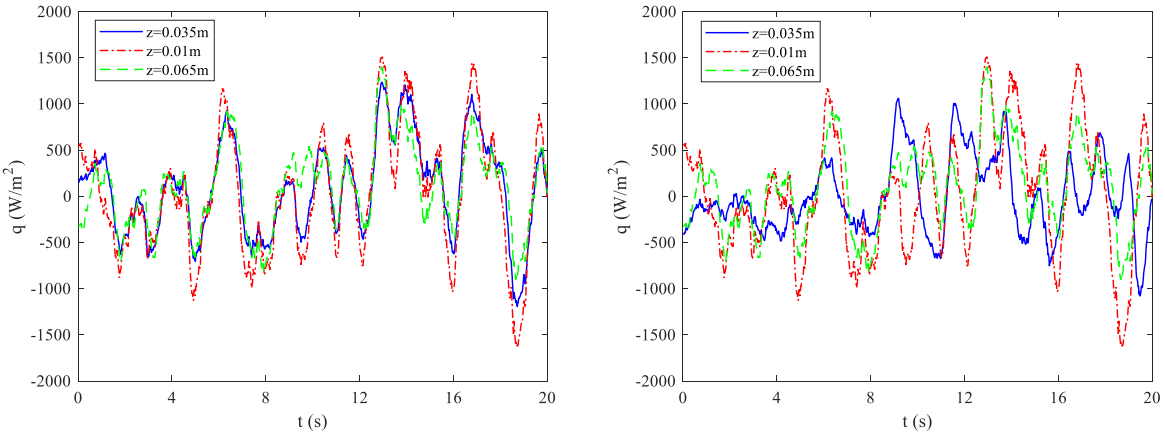

Figure 14. Heat flux distributions for the case of heat load of 100 W for the tube N°5 (a) and the tube N°7 (b).

Negative heat fluxes instead denote flow reversals phenomena during which the cold flow comes from the condenser at a lower temperature than the wall that was previously heated by hot fluid coming from the evaporator. From figure 13 the characteristic oscillating behaviour of the PHP is evident. Evaporative phenomena and flow reversals alternate with a dominant frequency (i.e. around 1 Hz) and with an average amplitude between 1500 and 2000 W/m^2.

Figure 14 shows the heat flux distributions obtained for other two channels (i.e. tubes N°5 and 7) for the three axial coordinate values considered in figure 13. It is possible to notice that the heat flux distributions are very close to the ones obtained for Tube N°3: this fact highlights that the oscillating behaviour that characterise the PHP involves all the channels with replicable characteristics demonstrating therefore the full activation of the device.

Moreover, in figure 14a it could be seen that the three distributions are in phase with an oscillation amplitude that is decreasing from the evaporator to the condenser (from z=0.01 m to z=0.065m): it seems that the fluid oscillates from the evaporator to the condenser for the whole length of the investigated section. In figure 14b instead it seems that there is a phase shift between the various positions indicating that there are oscillations of smaller amplitudes that do not necessarily affect the whole length of the analysed channel before changing direction.

In figure 15 the heat flux distributions obtained for other two values of heat loads (i.e. 34 W and 202 W) are reported. The heat flux distributions obtained for Channels N° 3,5,7 at axial coordinate z=0.035m are shown.

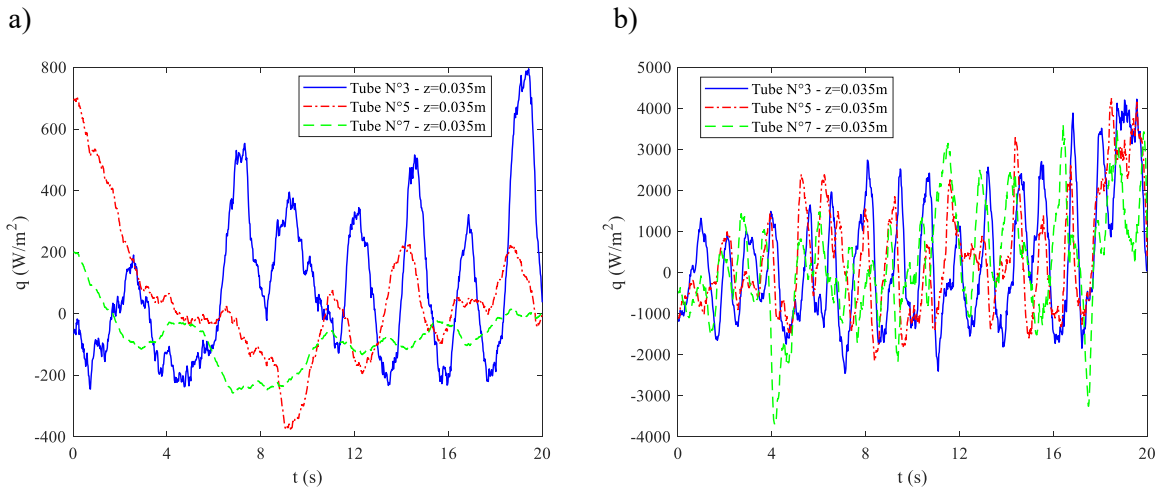

Figure 15. Heat flux distributions for the case of heat load of 34 W (a) and of 202 W(b).

For low power inputs (see figure 15a), the device response differs from channel to channel; in fact, some channels present an oscillating behaviour (Tube N°3), others show slight fluid movement interspersed with moments of inactivity (Tube N°5) while other channels (Tube N°7) are almost inactive, except for some weak oscillations. This means that the power input is not able to thermally drive the fluid in the whole device, thus the PHP is not yet fully activated. The overall operation regime can be classified as quasi-intermittent in micro-gravity conditions at this low heat power input.

On the contrary, for power input equal to 202 W (see figure 15b), the fluid oscillation is thermally induced in every channel and the device is fully activated. The oscillations result in high heat flux amplitudes and frequencies. In this case the regime is pure oscillatory and represents the test condition with best performance among those investigated.

6. Conclusions

In the present study an inverse analysis technique is applied to experimental infrared temperature data to estimate the local convective heat flux for forced convection flow inside Pulsating Heat Pipes. A PHP

specifically designed to be hosted on board the heat transfer host of the International Space Station was tested in microgravity during a Parabolic Flight Campaign.

The estimation procedure was firstly validated with synthetic data obtaining satisfactory results. Then, it was applied to experimental data obtained for different power input conditions. It was found that for low power inputs the PHP is not yet fully activated presenting different behaviours for each channel. The overall operation regime can be classified as quasi-intermittent in micro-gravity conditions. On the contrary, for higher power inputs (i.e. 100 W and 202 W) the fluid oscillation is thermally induced in every channel and the device is fully activated. In these cases, the regime is pure oscillatory.

Acknowledgments
The Authors would like to acknowledge UK's Engineering and Physical Science Research Council support through the grant EP/P013112/1 as well as the ESA MAP Project INWIP and ESA MAP Project TOPDESS.

References

[1] Murshed S S and De Castro C N 2017 A critical review of traditional and emerging techniques and fluids for electronics cooling Renew. Sust. Energ. Rev. 78 821
[2] Mangini D, Mameli M, Georgoulas A, Araneo L, Filippeschi S and Marengo M 2015 A pulsating heat pipe for space applications: Ground and microgravity experiments Int. J. Therm. Sci. 95 53
[3] Promvonge, P., Heat transfer behaviors in round tubes with conical ring inserts. Energy Conversion and Management, Vol. 49. 2008; 8-15
[4] H. Akachi, Structure of a heat pipe. US Patent 4,921,041, 1990
[5] De Paiva K V, Mantelli M B, Slongo L K, Burg S J, Gohr Jr R and Nicolau V. B. 2010 Experimental tests of mini heat pipe, pulsating heat pipe and heat spreader under microgravity conditions aboard suborbital rockets *Proc. of the 15th IHPC*, Clemson, South Carolina, USA.
[6] Rittidech S, Terdtoon P, Murakami M, Kamonpet P and Jompakdee W 2003 Correlation to Predict Heat Transfer Characteristics of a Closed-End Oscillating Heat Pipe at Normal Operating Condition Appl. Therm. Eng. 23 497
[7] Ma H 2015 Oscillating heat pipes (Berlin: Springer) 146
[8] Taft B S, Williams A D and Drolen B L 2012 Review of pulsating heat pipe working fluid selection J. Thermophys. Heat Tr. 26(4) 651
[9] Zhang Y and Faghri A 2008 Advances and unsolved issues in pulsating heat pipes Heat Transfer Eng 29 20
[10] Nazari M A, Ahmadi M H, Ghasempour R, Shafii M B, Mahian O, Kalogirou S and Wongwises S 2018 A review on pulsating heat pipes: from solar to cryogenic applications Appl Energy 222 475
[11] Beck, J. V., Blackwell, B., St Clair Jr, C. R., Inverse Heat Conduction: Ill-Posed Problems, A Wiley-Interscience, New York; 1985.
[12] H.R.B. Orlande, F. Olivier, D. Maillet, R.M. Cotta, Thermal measurements and inverse techniques, Taylor and Francis, New York , 2011.
[13] O. M. Alifanov, Inverse Heat Transfer Problem, Springer, Berlin, 1994.
[14] Chen, W. L., Yang, Y. C., Chang, W. J., & Lee, H. L. (2008). Inverse problem of estimating transient heat transfer rate on external wall of forced convection pipe. Energy conversion and management, 49(8), 2117-2123.
[15] Wu, L. W., & Yang, Y. T. (2005). Estimation of unknown outer-wall heat flux in turbulent circular pipe flow with conduction in the pipe wall. International journal of heat and mass transfer, 48(19-20), 3971-3981.
[16] Chen, W. L., Yang, Y. C., & Lee, H. L. (2009). Three-dimensional pipe fouling layer estimation by using conjugate gradient inverse method. Numerical Heat Transfer, Part A: Applications,

55(9), 845-865.
[17] Su, Antônio José da Silva Neto, J. (2001). Simultaneous estimation of inlet temperature and wall heat flux in turbulent circular pipe flow. Numerical Heat Transfer, Part A: Applications, 40(7), 751-766.
[18] Su, J., & Hewitt, G. F. (2004). Inverse heat conduction problem of estimating time-varying heat transfer coefficient. Numerical Heat Transfer, Part A: Applications, 45(8), 777-789.
[19] Cattani, L., Mangini, D., Bozzoli, F., Pietrasanta, L., Mameli, M., Filippeschi, S., ... & Marengo, M. (2019). An original look into pulsating heat pipes: Inverse heat conduction approach for assessing the thermal behaviour. Thermal Science and Engineering Progress, 10, 317-326.
[20] A.N. Tichonov, V.Y. Arsenin, Solution of Ill-Posed Problems, Winston & Sons, Washington; 1977
[21] Cyganek, B., & Siebert, J. P. (2011). An introduction to 3D computer vision techniques and algorithms. John Wiley & Sons.
[22] Astarita, T., & Carlomagno, G. M. (2012). Infrared thermography for thermo-fluid-dynamics. Springer Science & Business Media.
[23] Mameli, M., Catarsi, A., Mangini, D., Pietrasanta, L., Michè, N., Marengo, M., ... & Filippeschi, S. (2019). Start-up in microgravity and local thermodynamic states of a hybrid loop thermosyphon/pulsating heat pipe. Applied Thermal Engineering, 158, 113771.
[24] Incropera, F. P., DeWitt, D. P., Bergman, T. L., & Lavine, A. S. (1996). Fundamentals of heat and mass transfer (Vol. 6, p. 116). New York: Wiley.
[25] Bozzoli, F., Cattani, L., Rainieri, S., Bazán, F.S.V. and Borges, L.S.,Estimation of the local heat transfer coefficient in coiled tubes: Comparison between Tikhonov regularization method and Gaussian filtering technique, International Journal of Numerical Methods for Heat and Fluid Flow 27(2018) 575-586.
[26] Hansen, P. C., and O'Leary, D. P., The use of the L-curve in the regularization of discrete ill-posed problems. SIAM journal on scientific computing, Vol. 14(6). 1993; 1487-1503.